International Journal of Fracture (2005) 131:35–52
DOI 10.1007/s10704-004-3177-z

Observed and simulated fracture pattern in diametrically loaded discs of rock material

B. VAN DE STEEN[1], A. VERVOORT[1,*] and J.A.L. NAPIER[2]
[1] *Catholic University Leuven, Kasteelpark Arenberg 40, 3001 Leuven, Belgium*
[2] *School of Computational and Applied Mathematics, University of the Witwatersrand, Johannesburg, South Africa*
[*] *Author for correspondence (E-mail: andre.vervoort@bwk.kuleuven.ac.be (Vervoort))*

Received 26 January 2004; accepted in revised form 10 September 2004

Abstract. To investigate the influence of a tensile stress gradient on fracture initiation and fracture growth in rock material, a configuration, consisting of a diametrically loaded disc with a hole on the diameter perpendicular to the loaded diameter, is used. The maximum local tensile stresses the material is able to withstand increase as the stress gradient increases. Depending on the diameter and the eccentricity of the hole, the disc splits along the loaded diameter or macro-fracturing starts at the hole. However, the tensile stresses at the top and the bottom of the hole are for nearly all cases considerably higher than the stress along the loaded diameter and than the macroscopic tensile strength of the material, determined by conventional Brazilian tests. To better understand this particular fracturing behaviour, numerical simulations of the experiments are conducted using the boundary element code DIGS, which allows the incorporation of weak elements (flaws), representing defects and weaknesses in the rock material. It is shown that the influence of the stress gradient on the stress concentration at the tip of mobilised defects lies at the origin of the particular fracturing behaviour in the diametrically loaded disc with a hole. The study of the new configuration leads also to a number of conclusions with regard to the failure in diametrically loaded discs in general. Based on the flaw model, fracture initiation in the Brazilian test has to be attributed to fracture growth of a mobilised defect, situated in the area close to one of the platens.

Key words: Boundary element method, Brazilian test, Displacement discontinuity method, rock testing, size effect, tensile stress gradient.

1. Introduction

Stress gradients induced by excavations in rock depend on the configuration and the size of the excavation and on the loading conditions. For the same pre-excavation in situ stresses, the stress gradients around, e.g., a circular 5-m diameter tunnel or around a 32-mm drill hole differ considerably: the stress pattern is self-similar but obviously, for the smaller hole, the stress reduces to the field stress over a shorter distance. Similarly, the stress gradients at the corners of a rectangular tunnel differ considerably from the stress gradient around a circular tunnel. Stress gradients not only occur on the macro-scale but also on a micro-scale. High stress gradients exist in the vicinity of flaws, at grain contacts or at pores in the material.

In this study, attention is focused on the influence of a tensile stress gradient on fracture initiation and fracture growth in brittle rock. To investigate the response of the rock to a stress gradient, a number of tests involving a tensile stress gradient were evaluated (Van de Steen, 2001), but prior to this evaluation an overview is given on size effect theories, frequently associated with stress gradients. These size effect theories can be subdivided in three categories (Sellers, 1999): energy methods, statistical theories and non-local theories of stress and strain.

The fundamental assumption of the energy approach to fracture growth (e.g., Bažant, 1984; Bažant and Kazemi, 1990) is that a fracture grows as strain energy from the zones next to the fracture is relieved into the fracture front. A size effect arises because the released energy is proportional to the volume of the material and the fracture energy is proportional to the fracture area. The theory requires the presence of a crack before reaching the maximum load, and the theory is therefore not applicable to describe fracture initiation, as recognised by Bažant and Li (1995).

The concept that a randomness in strength characteristics influences the response of a specimen or structure is not disputed by most researchers. Strength deviations from the mean strength are observed to decrease with increasing sample size (Martin, 1997). Attributing the size effect to a randomness of the intrinsic material strength only, has however drawn more criticism (Swan, 1980; Bažant and Chen, 1997). It is argued that the Weibull-type theories cannot be applicable to rocks in general because they do not allow for a stress redistribution due to cracking either for crack coalescence or for the development of a fracture process zone. The statistical approach of Carpinteri et al. (1997) links the variability of the tensile strength to the probability density of the crack size distribution. Smaller structures exhibit a larger spread in the results, but are stronger, while larger structures fail at lower stresses, but are less variable.

The observation that the fracture surface roughness can be described by fractal concepts led to the multi-fractal approach of fracturing. A fractal energy concept (Borodich, 1999) had to be introduced to limit the energy required to extend a fractal crack to finite values.

In the non-local theories, the stress at a point is generally a function of the mean of the (equivalent) strain over a certain representative volume, area or line at that point (Pijaudier-Cabot and Bažant, 1988). It is clear that non-local theories always involve the introduction of a characteristic length scale, to be considered as a material parameter. Closely related to the non-local damage models are the gradient enhanced damage models. In these models the integral equation is approximated by a partial differential equation and, for example, implemented in a finite element code (de Borst et al., 1995). Probabilistic non-local damage models (Carmeliet and Hens, 1994; Carmeliet and de Borst, 1995) exhibit both a deterministic and a probabilistic size effect. As the size of the specimen increases, the stress at failure decreases and the variability in the results decreases.

The stress gradient theory (Lajtai, 1972; Nesetova and Lajtai, 1973; Carter, 1992) is a non-local stress approach to fracturing. A linear elastic stress analysis is carried out, after which the stress is averaged along the fracture path. The averaged stress is then evaluated against the failure criterion. The researchers supporting this approach argue that most stress fields are highly inhomogeneous in detail, and that

even in brittle materials, the material transfers the high stresses into regions of lower stress, effectively averaging the stress gradients over a distance δ, where δ is a material parameter.

In this paper, a series of numerical simulations of the fracturing in a diametrically loaded disc containing a hole shows how the fracture pattern is controlled by the size of the hole in the presence of material defects.

2. Rock studied

The rock for which the results are reported in this paper is a crinoidal limestone. It contains approximately 35% crinoids embedded in a micrite matrix. Each crinoid fragment is a single calcite crystal. Although crystals with a diameter of up to 7 mm are observed, their diameter typically varies between 60 and 400 μm (Van de Steen et al., 2002). The micrite, very fine-grained calcite, is the second major constituent of the crinoidal limestone. The rock further contains some other bioclast. As in most carbonate rocks, the dominant mineral is calcite, accounting for approximately 96–99% by weight of the rock content. There are traces of dolomite as is the case in most limestones. Other secondary minerals include finely dispersed microcrystalline quartz and iron sulphides, while the stylolites that are frequently encountered in the rock may also contain organic material and clay minerals. Samples containing dominant stylolite bands were rejected for testing. In view of its response to fracturing, the granular nature of the material as well as its internal structure (cleavage planes), the presence of different types of defects and weaknesses in the material (e.g., stylolites, voids, grain boundaries), together with the applied stress field, govern the fracturing in the material (Van de Steen, 2001; Van de Steen et al., 2002).

3. Sample configuration and observations

In the Brazilian test configuration, a disc is loaded diametrically, inducing an almost uniform tensile stress in the direction perpendicular to the loading along most of the loaded diameter. When a hole is drilled parallel to the sample axis, and centred on the diameter perpendicular to the loaded diameter (a configuration further referred to as the disc with a hole, Figure 1), the material above and below the hole is subjected to a rapidly decreasing tensile stress. A linear elastic analysis of the stress distribution shows that the maximum tensile stresses at the hole surface decrease as the distance between the centre of the disc and the centre of the hole (termed the eccentricity, e) increases (Figure 1). It was further shown that an increase in the radius a of the hole leads to a decrease in the stress gradient (Van de Steen, 2001; Van de Steen and Vervoort, 2001). Except for small holes ($a/R \leq 0.08$) in combination with a large eccentricity ($e/R \geq 0.8$), the tensile stress at the top and the bottom of the hole is larger than the tensile stress along the loaded diameter. For example, for a 50-mm diameter disc with a 4-mm diameter hole ($a = 2$ mm) and an eccentricity of 8 mm, the tensile stress at the hole is about four times the tensile stress along the loaded diameter. Figure 2 shows the experimental results of the effect of the eccentricity and the hole radius on the location of failure at either the hole surface or along the loaded diameter. It appears from Figure 2 that the failure occurs over the loaded diameter if the eccentricity of the hole is increased sufficiently.

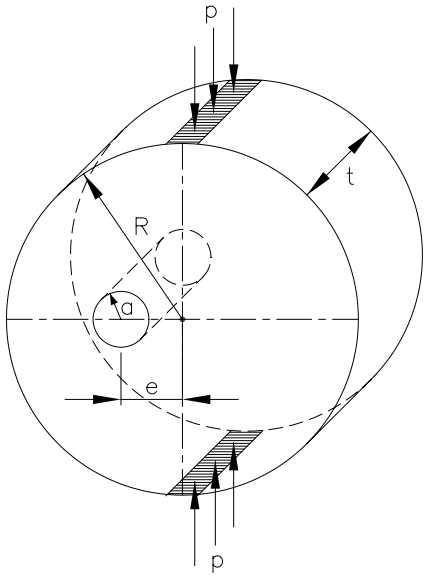

Figure 1. Diametrically loaded disc with a hole: geometrical configuration.

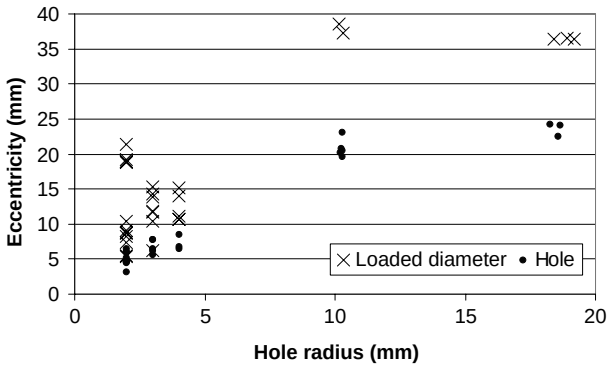

Figure 2. Experimental results of the influence of eccentricity and hole radius on the fracturing behaviour (along the loaded diameter or at the hole surface).

A typical unstable fracture along the loaded diameter and a stable fracture growing from the hole towards the platen contacts are presented, respectively, in Figures 3 and 4. To indicate the onset of damage in the vicinity of the hole, cotton wool saturated with water was inserted in the hole; the capillary rise of water serves as an indication of damage initiation and development (Figure 4). There was no sign of any capillary action near the hole in the disc that split along the loaded diameter (Figure 3). Hence, if any possible damage occurred, it remained limited.

During the test, the acoustic emission was recorded as well (Figures 5 and 6). For the sample that split along the loaded diameter (Figure 3), most of the activity was centred around the loaded diameter (Figures 5a and 5b), with no additional activity around the hole. While acoustic activity below the detection threshold obviously does not show up directly on the figures, it is argued that the time–position plot (Figure 5b) nevertheless provides an indication that the low energy cracking must also remain minimal for the following reasons. Although their acoustic activity might not be dis-

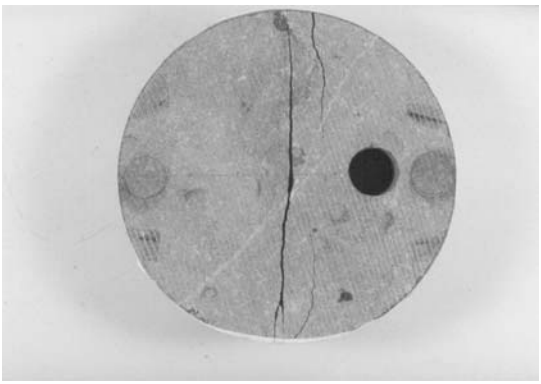

Figure 3. Diametrically loaded disc with hole, split along the loaded diameter without intersecting the hole.

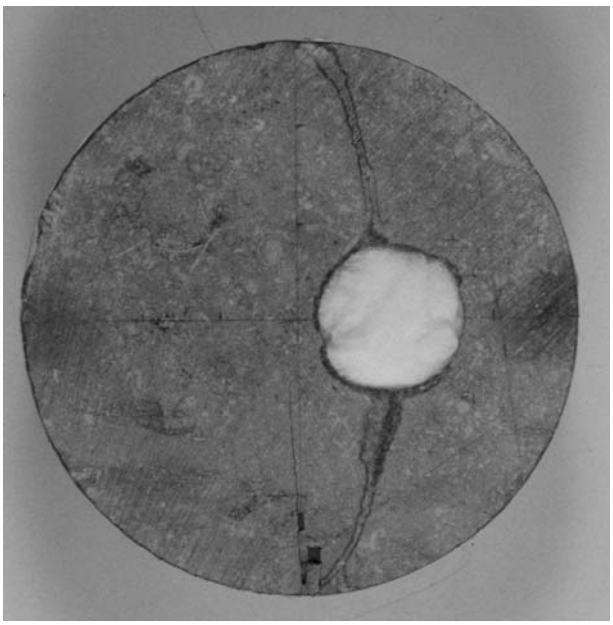

Figure 4. Diametrically loaded disc with hole with the primary fractures intersecting the hole and a secondary fracture growing from the bottom platen contact to the centre of the disc.

cernible from the noise, the activation of a large number of low energy micro-fractures would reduce the Young's modulus of the material, and hence reduce the speed of the elastic waves (Couvreur, 1997). The reduction in the wave velocity would then show up in the time–position diagram as an increasing offset of the activity originating from the centre, in a direction away from the hole. This is clearly not the case, which warrants the conclusion that the damage in the vicinity of the hole remains negligible or, at least, limited.

In the disc that fails at the hole (Figures 4 and 6), the acoustic emission clearly shows the fracture initiation and growth process, while the activity in the centre of the disc remains very limited until the primary fractures have almost reached the platen contacts. The apparent position histogram seems to consist of two

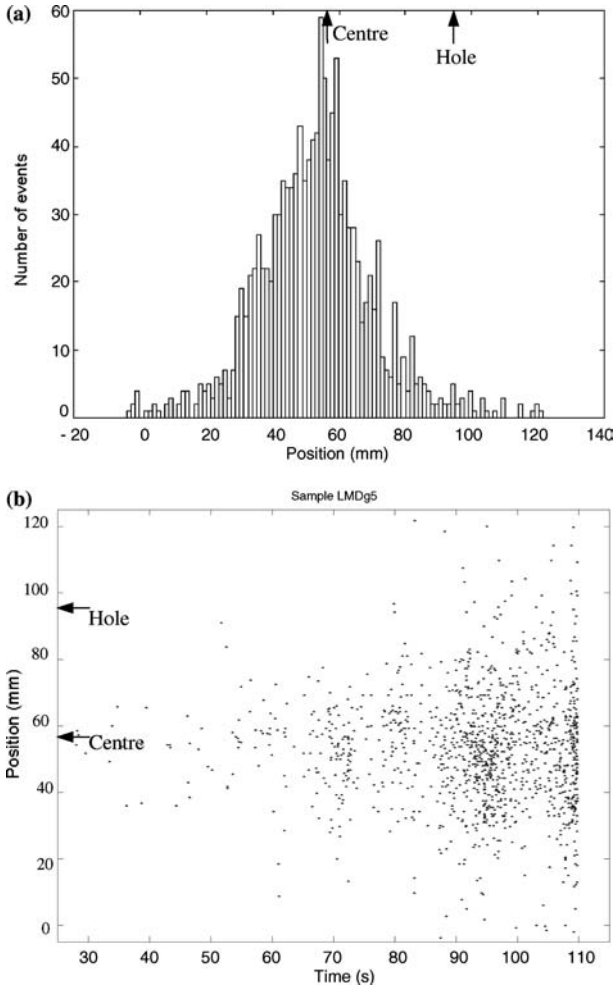

Figure 5. Acoustic emission activity registered during the loading of a diametrically loaded disc with a hole that fractured along the loaded diameter without intersecting the hole. (a) Number of events as function of the position. (b) Time–position plot.

sub-populations marked a and b in Figure 6a: one to the left and one to the right of the hole. The appearance of these two sub-populations (instead of one single peak) is an artefact induced by the presence of the hole. All events originate in the vicinity of the hole, either above or below it. However, events occurring close to the hole are shielded from one of the two sensors that are placed on the horizontal diameter, close to the disc boundary. The shielding results in an apparent position that is shifted to the left or to the right, away from the sensor from which they are shielded. To verify the hypothesis about the origin of the two sub-populations, the actual tests were preceded by a calibration stage in which small excitations (induced by breaking pencil leads on the surface of the sample) were introduced in pre-determined positions (Hsu and Hardy, 1978). This procedure confirmed that the presence of the hole introduces an apparent shift of the source, away from the shielded sensor. The narrow cloud of points marked C in Figure 6b corresponds to the broad AE activity zone marked c in Figure 6a. This activity is due to a secondary fracture that extends

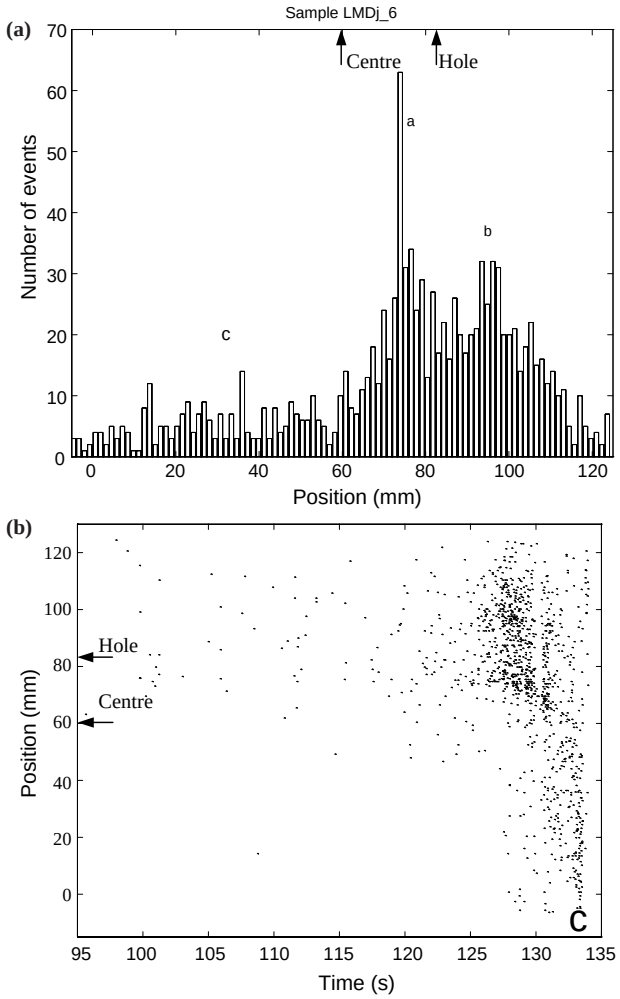

Figure 6. Acoustic emission activity registered during the loading of a diametrically loaded disc with a hole with the fracture initiated at the hole surface. (a) Number of events as function of the position. (b) Time–position plot.

from the bottom platen contact to the centre of the disc (Figure 4). The large offset and the wide range in which the activity is apparently situated, is a consequence of the damage associated with the fracture from the hole to the bottom platen through which the elastic waves have to travel to reach the second sensor and which reduces the effective wave propagation speed considerably.

The acoustic emission measurements and the capillary action indicate that when the nominal tensile strength of the material is exceeded at the hole surface, this does not necessarily give rise to damage or extensive cracking. The fracture does not appear to form unless the load is distributed over a sufficiently extensive distance or area. Locally, the material can withstand stresses that are several times the nominal tensile strength. The behaviour described above was not only observed in crinoidal limestone, but also in sandstone, in porphyry and in mortar samples (Van de Steen, 2001). In the mortar samples, the hole was formed during the casting of the mortar to avoid damage being caused during the drilling of the hole.

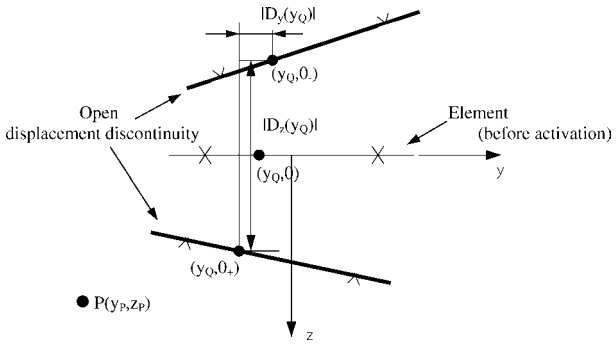

Figure 7. Schematic representation of a linearly varying displacement discontinuity element having two internal collocation points. The original, closed element and the position of the two sides of the displacement discontinuity surfaces after activation are indicated.

4. Model and implementation

To represent the nature of the material completely, a micro-mechanical model aimed at describing the fracture initiation and fracture growth, should probably take the granular nature, the internal structure of the grains and the presence of the defects and weaknesses present in the rock all into account. To study the interaction of cracks and fractures and to model the transition of the intact material (continuum) to the failed material (discontinuum), cracks and fractures should be modelled explicitly. The boundary element code DIGS (Discontinuity Interaction and Growth Simulation; Napier, 1990; Napier and Hildyard, 1992; Malan and Napier, 1995; Napier and Peirce, 1995; Napier et al., 1997; Napier and Malan, 1997) allows the aforementioned features to be implemented, although the simulations presented here focus on the presence of defects and weaknesses. DIGS is a two-dimensional code based on the displacement discontinuity method (Crouch and Starfield, 1983). In an elastic solid, the displacements are assumed to be continuous, except over the discontinuity elements that model both the boundary of the problem (hole and circumference of disc) and the internal cracks and fractures. All non-linear effects in the model are contained in and reflected by the displacement discontinuities; the host material remains linear elastic. Over straight-line elements with normal vector components n_y and n_z, centred on the y-axis of a local co-ordinate system y–z (Figure7) and length $2b$, the local displacement discontinuity components are defined as:

$$D_i(y_Q) = u_i(y_Q, 0_-) - u_i(y_Q, 0_+) \quad i = y, z; -b \le y_Q \le b \tag{1}$$

where $z = 0_+$ designates the positive side and $z = 0-$ the negative side of the discontinuity surfaces with respect to the local normal (positive z-axis). The displacement discontinuity vector components, D_i, are evaluated at two collocation points within each element to ensure that the appropriate crack sliding or opening stress boundary conditions are satisfied (Napier and Malan, 1997; Crawford and Curran, 1982). The total stress value at any point P is determined by summing the contributions of all discontinuity elements defining the sample and hole boundaries and the cracks and fractures within the material (Napier and Malan, 1997).

Fractures in rock are often determined by the granular nature of the material and by the internal structure of its composing minerals. Random mesh grids can be used as an approximate representation of some of these features. For example, Voronoi polygons are reminiscent of granular rock particles (Figure 8a). The internal structure of the minerals can be represented by subdividing each polygon into triangles by connecting the vertices of each polygon to the geometric centre (Figure 8b). Each of the edges of these triangles is assigned a failure criterion and a set of matching strength properties. A subset of these edges, designated as *flaws*, is selected at random and assigned reduced strength properties. In a particular numerical experiment, loading steps are applied to the sample platens and crack slip and opening displacements are computed at all active crack element collocation points. The initiation of new fractures is reviewed at the end of each loading step by computing stress values at the collocation points of 'intact' elements (candidate crack elements not yet mobilised). One or more of the elements, for which the failure criterion is exceeded at, at least, one of the two collocation points, is then activated according to a pre-defined priority rule. For a given applied load, the interacting displacement discontinuities undergo both sliding and opening movements, which are calculated through an iterative solution scheme. Since they have reduced strength properties, it is evident that the flaws are the first elements to be activated in the zones with the most critical stress conditions.

The material studied here is a typical granular material with a large variation in grain size (from crystals of up to 7 mm to very fine grained ($< 4\,\mu$m) calcite in the micrite). The aim of the simulations presented here is not to incorporate this complex granular structure in all its details into the model. However, the natural weaknesses and defects are indirectly incorporated into the model by giving reduced strength properties to certain elements (called *flaws*).

5. Simulations

5.1. Fracture pattern

The model was applied to two test cases corresponding to the laboratory tests where fracturing was observed to occur consistently along either the loaded sample

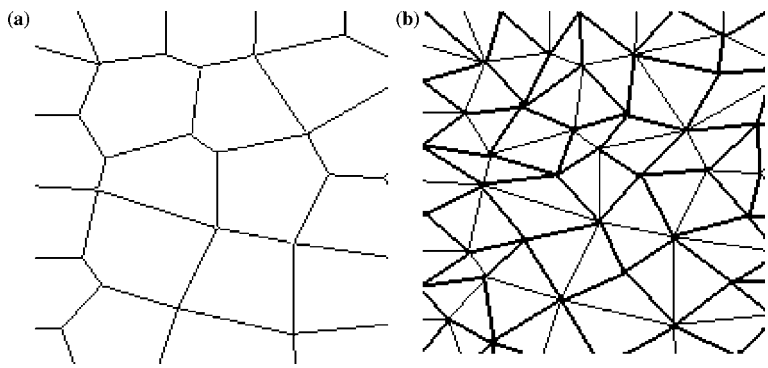

Figure 8. Voronoi tessellation (a) and Voronoi tessellation with internal fracture paths (b).

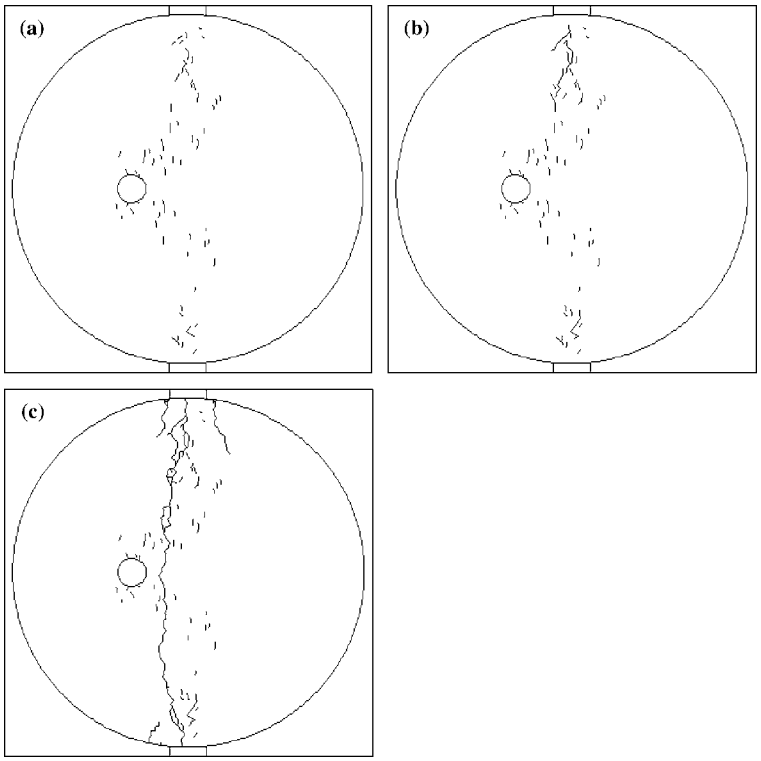

Figure 9. Fracture formation in a diametrically loaded disc with a 'small' hole.

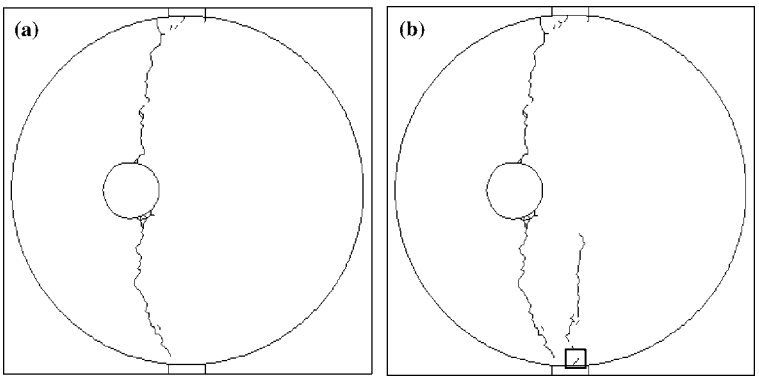

Figure 10. Fracture formation in a diametrically loaded disc with a 'large' hole. The fracture starting from the bottom of the sample and growing towards the centre nucleates in shear in the enclosed region.

diameter or from the hole surface. In particular, the 50-mm diameter discs, in which a 4-mm hole is drilled with an eccentricity of 8 mm, failed consistently along the loaded diameter and the 50-mm diameter discs, in which a 8-mm hole is drilled with an eccentricity of 8 mm, failed at the hole surface. The 4-mm holes are further called the 'small' holes, whereas the 8-mm holes are called the 'large' holes. The fracture patterns generated by these simulations are shown in Figures 9 and 10. The element and flaw properties are given in Table 1. A Voronoi tessellation with internal fracture

Table 1. Material properties and model characteristics used in the simulation of the discs with a hole.

	Figure 9 ('small' hole)	Figure 10 ('large' hole)
Tension cut-off intact elements	35 MPa	35 MPa
Cohesion intact elements	80 MPa	80 MPa
Tension cut-off flaws	7 MPa	7 MPa
Cohesion flaws	25 MPa	25 MPa
Flaw density	12.5%	12.5%
Unmobilised friction angle	35°	35°
Residual friction angle	20°	20°
Dilatation angle	15°	15°
Ratio average element length to disc radius	0.0278	0.0278
Total number of elements	9690	9366

paths was used to mesh a central band with width R, equal to the sample radius. The same strength properties were assigned to the internal fracture paths and to the Voronoi boundaries.

In the initial stage of fracture, shown in Figure 9a ('small' hole), a number of flaws are activated under the applied load in the regions of high tensile stress, and in the region situated about $0.2R$ under the top platen and above the bottom platen. Whereas the failure mode in the region of high tensile stress is exclusively tensile, the failure in the latter areas is predominantly shear-driven. In the next phase, a number of activated flaws in the area $0.2R$ under the top platen start to coalesce to form fractures (Figure 9b). In the course of this process, failure occurs in both shear and tension. As the diametrical fracture develops, tensile failure becomes the dominating mechanism. Once the primary fracture has fully developed, secondary, almost vertical tensile fractures start to grow from the edge of the disc (Figure 9c). Apart from the initial flaw activation, no additional fracturing occurs in the region of the stress concentrator.

In Figure 10, the sample with the 'large' hole, only a few flaws are activated before the macro-fractures start to develop. The fracturing process is totally dominated by the tensile failure of elements in the vicinity of the hole. The activated elements immediately grow into a macro-fracture. Shear failure plays a marginal role in the development of the fractures emanating from the hole (Figure 10a): the only elements forming part of these fractures that fail in shear are the elements close to the platens. Before the fractures that started from the hole reach the edge of the disc, a number of elements fail in shear just above the bottom platen, to form the start of a fracture along the loaded diameter. This fracture extends from the bottom platen to approximately the centre of the sample (Figure 10b). These types of fractures were also observed in some of the samples that failed at the hole in the laboratory experiments (see, e.g., Figure 4).

5.2. Fracture initiation: mechanism

The numerical simulations suggest that the fracture splitting the disc is initiated at an activated flaw, close to the platen contact, and that both the mobilisation of the flaws

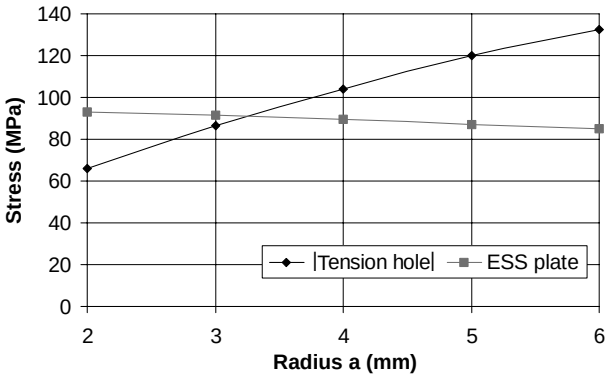

Figure 11. Absolute values of the normal stress, at a distance of 0.1 mm in front of a 0.7-mm crack at the hole surface and excess shear stress (ESS), at a distance of 0.1 mm in front of a 0.7-mm crack under the platen. Values are plotted as a function of the hole radius for a fixed disc with a radius, $R = 25$ mm and hole eccentricity, $e = 8$ mm. The sample is loaded with a line load of 1060 N/mm.

that are activated in the platen region and the initial fracture growth are shear-driven. The fracture at the hole, on the other hand, is initiated at a flaw that was mobilised in tension and the fracture growth process is in tension. Since the presence of cracks can give rise to important stress concentrations, the concept that defects are mobilised prior to macro-fracture growth implies that the stresses that the 'intact' material can withstand are considerably higher than the nominal stresses that the rock as a whole can resist. The tension cut-off and the cohesion of the intact elements should therefore not be compared to the macroscopic tensile strength or the macroscopic cohesion, which are values that result from an interaction between the defects and the intact material.

To understand the difference in fracturing in the disc with the 'small' hole and the disc with the 'large' hole, the stress concentrations at the tip of the crack have to be considered. Crack growth is determined either by the magnitude of the tensile stress in front of the crack tip, in a direction perpendicular to the prospective fracture path or, from the Coulomb criterion, by the 'excess shear stress' (ESS) in the direction of the prospective fracture path. The ESS is defined as $\mathrm{ESS} = |\tau| - \sigma_n \tan\varphi$, where τ is the shear stress in the growth direction, σ_n the normal stress perpendicular to the growth direction ($\sigma_n < 0$ is tensile) and φ the unmobilised friction angle. The tensile stress has to be compared to the tension cut-off and the ESS to the cohesion. In Figure 11, the normal tensile stress in front of a crack at the hole and the ESS around a crack a few millimetres under the top platens are given as a function of hole radius (overall disc radius $R = 25$ mm; crack length $2b = 0.7$ mm; stresses at 0.10 mm from the crack tip; diametrical load equivalent to a line load of 1060 N/mm). The crack at the hole is oriented parallel to the applied load, while the crack under the platen makes an angle of 30° with the applied load. The tensile stress in front of the crack tip, emanating from the hole, increases as the hole radius increases. The ESS in front of a crack under the platen on the other hand decreases slightly with an increase in hole diameter.

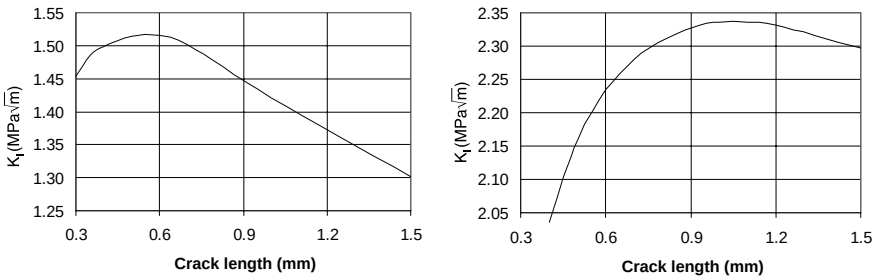

Figure 12. Mode I stress intensity factor above a 'small' hole (left; $a = 2$ mm) and above a 'large' hole (right; $a = 4$ mm). The distributed load is equivalent to a line load $W = 982$ N/mm.

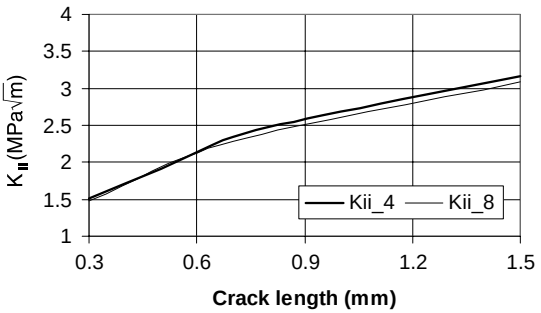

Figure 13. Mode II stress intensity factor near the platens in a disc with a 'small' ($a = 2$ mm) and with a 'large' hole ($a = 4$ mm). The distributed load is equivalent to a line load $W = 982$ N/mm.

5.3. Stress intensity factors

The calculation of the stress intensity factor K_I at the hole confirms that after an initial unstable fracture initiation process, further fracture growth becomes stable. Near the platens, the whole process is unstable as indicated by the evolution of K_{II}. The stress intensity factors K_I at 4- and 8-mm diameter holes, and the stress intensity factor K_{II} close to the platens for both hole diameters are given in Figures 12 and 13, respectively. In each case, the crack grows in its own plane; i.e., vertically for the crack from the hole surface, and at an angle of 30° for the crack close to the platens. The shape of the K_I curves (Figure 12) indicates that the fracture initiation process is unstable. However, the K_I curves reach a maximum value. At the 'small' hole, the maximum K_I value is not only lower than at the 'large' hole, it is also reached for smaller crack lengths. Moreover, the stress intensity factor decreases faster with an increase in crack length at the 'small' hole. This implies that fracture initiation at 'large' holes easily leads to the development of a macro-fracture. The K_{II} value near the platens on the other hand does not have a maximum, but increases with an increasing crack length; crack growth in this area is therefore unstable for the range of crack lengths shown in Figure 13.

6. Brazilian test

It appears that the formation of a primary diametrical fracture (for holes with sufficiently large eccentricity) or a secondary diametrical fracture, following primary

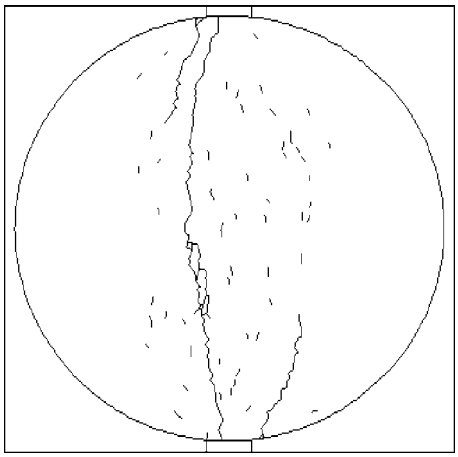

Figure 14. Fracture pattern obtained with a tension only (Rankine) failure criterion in the conventional Brazilian test.

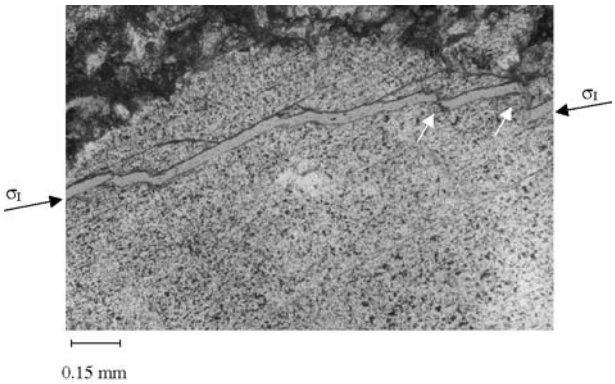

Figure 15. Fracture path with a discontinuous aspect (conventional Brazilian test). The fracture follows a number of different cleavage planes over part of its trajectory and has a distinct step-wise (= *en echelon*) aspect.

fracturing from the hole surface, are initiated by shear fracturing close to the platen contact with the sample. These observations immediately raise questions about the fracture initiation mechanism in the conventional Brazilian test (without a hole). There is little or no discussion that the fracture grows in tension. However, there is more controversy about the initiation mechanism and location (Hondros, 1959; Fairhurst, 1964; Colback, 1966; Mellor and Hawkes, 1971; Hudson et al., 1972; Falls et al., 1991; Clatworthy et al., 1993).

Colback (1966) argued that a curved fracture path points to fracture initiation in shear near one of the platens. However, the DIGS simulations indicate that the fracture pattern as such cannot be used to determine whether the fracture initiates in tension or in shear (Van de Steen, 2001). When the fracture path is strictly diametrical, a shear mechanism can still be responsible for fracture initiation, and a curved fracture path does not necessarily point to a fracture that was initiated in shear. The curved primary fracture shown in Figure 14 is obtained with a tension only (Rankine) failure criterion. The flaws that are activated in the initial loading stages dominate the frac-

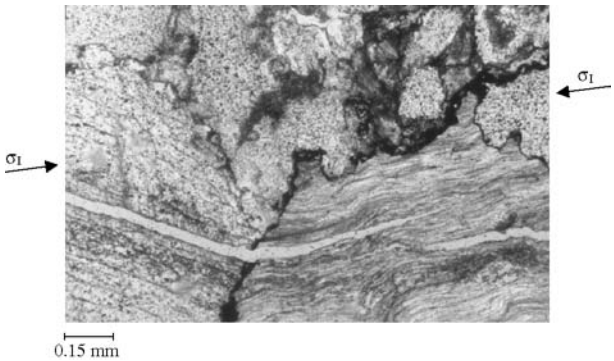

Figure 16. Main fracture forming an *en echelon* pattern in a shell fragment (conventional Brazilian test).

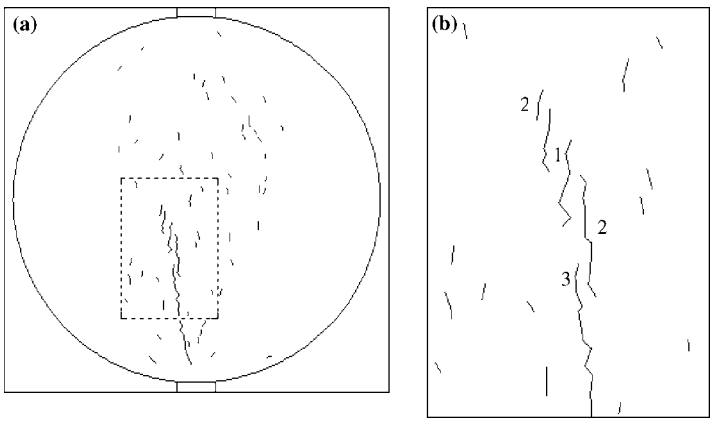

Figure 17. Formation of an *en echelon* pattern in the Brazilian test (see also Figure 14). 1: The first two sub-fractures form independently at an early stage from flaws and intact elements. 2: The existing sub-fractures activate flaws in front of the crack tip. These flaws grow immediately into sub-fractures. 3: An already activated flaw starts to grow as the above-lying sub-fracture approaches.

turing rather than the general stress distribution that is obtained in a homogeneous, isotropic and crack free sample.

En echelon patterns, often associated with compressive stress fields, were also observed in discs subjected to the Brazilian test loading configuration. Examples of *en echelon* patterns before and after coalescence are shown in Figures 15 and 16. These two figures are photographs of thin slices prepared from a disc subjected to Brazilian test loading that was halted immediately when the failure load was reached. Without pulling the sample 'halves' apart, the sample was immersed in a resin and subsequently sectioned into thin slices. The occurrence of the step-like features shown in Figures 15 and 16 is, in both instances, associated with preferential fracture paths, i.e., weaknesses in the material. In Figure 15, the cleavage planes in the calcite crystal form the weakness and in Figure 16, the structure of the shell fragment provides a preferential fracture path.

The *en echelon* structure is also observed in the numerical simulations. In Figures 17a and 17b, the pattern that existed during the development of the primary fracture, but prior to the occurrence of the macro-fracture, is shown. The small isolated blocks

of material in Figure 14 (at a distance of about one-third of the diameter from the bottom platen), are formed by *en echelon* fracture patterns.

A proposed hypothesis for the origin of the above structures is that the stress concentration that exists in front of a growing fracture activates defects or weaknesses that are present in the vicinity of the advancing fracture tip, but are not necessarily connected to the growing tip. Once activated, further growth can occur from the newly mobilised crack segments, effectively leading to the patterns observed on the thin slices (see Figures 15 and 16) and also demonstrated in the simulations (e.g., Figure 17). In the simulation the two small fractures, located to the left and to the right of the position marked '1', formed independently of each other at an early stage and are made up of activated flaws and activated intact elements. At the failure load, they grew to the size shown in Figure 17b. The initial two small fractures activated flaws at their external fracture tips (see position '2' in Figure 17b). At the position '3', an already mobilised flaw started to grow as the above-lying fracture '2' approached, and fracture growth was carried over onto the external crack tip located in '3'. This eventually gave rise to the situation shown in Figure 17a. Coalescence of the different fragments occurs at a later stage of the fracture growth process (see Figure 14).

7. Conclusions

A diametrically loaded disc with a hole is a versatile, easy to prepare and easy to test configuration to study, in general, fracture initiation and growth in brittle rock, and more specifically the effect of a stress gradient. A change in the hole diameter and in the eccentricity of the hole position suffice to vary the tensile stress and the stress gradient at the hole surface. Depending on the hole position and diameter, the ratio of the elastically calculated tensile stress at the hole surface to the macroscopic tensile strength can reach values of four or more. Notwithstanding the high tensile stresses at the hole, it was experimentally observed that failure often occurs as a diametrical splitting of the disc without intersecting the hole.

The laboratory observations of the development of the fracturing in the disc with a hole were successfully simulated by the boundary element code DIGS. The code provides a framework for the approximate representation of the irregular, granular nature of rock and the presence of defects and weaknesses. The simulations demonstrate that the presence of pre-existing flaws serves to explain the effect of different hole sizes in the formation of primary fracture features either from the hole surface or in the form of a diametrical fracture that does not intersect the hole. If the stress gradient around the hole falls off rapidly away from the hole surface, the stress concentration at the tips of defects mobilised close to the hole decreases sufficiently to make the development of a macro-fracture from the edge of the hole less likely, and the discs fail along the loaded diameter instead. The effective 'loading stiffness' of the material surrounding potential cracks is probably greater near the hole surface than at the centre of the sample when the hole diameter is sufficiently small.

When failure occurs at the hole surface, fracture initiation and fracture growth are both tension-driven. The secondary fractures that are observed in these tests are also simulated. A fracture that either splits the sample diametrically or that extends from one of the platen contacts to the centre of the disc, is initiated in shear close to one of the platens while its subsequent growth is tension-driven. Fracture initiation in the

'classical' Brazilian test is believed to be controlled by a similar mechanism. Specifically, it is proposed that fracturing in the Brazilian test is initiated in shear in the vicinity of one of the platens, and subsequently grows in tension. In addition, flaws can be mobilised in front of a growing fracture, which may, for example, lead to the formation of *en echelon* patterns, as observed on laboratory samples, as well as in the simulations. This can explain why the diametrical macro-fracture is not a single continuous crack, but is built up of several coalesced fractures.

At the hole surface, fracture growth is initially unstable, but becomes stable as the fracture length increases. The mode I stress intensity factor increases to a maximum value as a function of the distance from the hole surface. The magnitude of the maximum value increases as the hole diameter increases. Conversely, shear fracture growth from the vicinity of the loading platen is an unstable process, with the mode II stress intensity factor increasing as the crack length increases.

References

Bažant, Z.P. (1984). Size effect in blunt fracture: concrete, rock, metals. *J. Eng. Mech. ASCE* **110**, 518–535.

Bažant, Z.P. and Chen, E.-P. (1997). Scaling of structural failure. *Appl. Mech. Rev*. **50**, 593–627.

Bažant, Z.P. and Kazemi, M.T. (1990). Determination of fracture energy, process zone length and brittleness number from size effect, with application to rock and concrete. *Int. J. Fract.* **44**, 111–131.

Bažant, Z.P. and Li, Z. (1995). Modulus of rupture: size effect due to fracture initiation in boundary layer. *J. Struct. Eng*. **121**, 739–746.

Borodich, F.M. (1999). Fractals and fractal scaling in fracture mechanics. *Int. J. Fracture* **95**, 239–259.

Carmeliet, J. and de Borst, R. (1995). Stochastic approaches for damage evolution in standard and non-standard continua. *Int. J. Solids Struct*. **32**, 1149–1160.

Carmeliet, J. and Hens, H. (1994). Probabilistic nonlocal damage model for continua with random field properties. *J. Eng. Mech. ASCE* **120**, 2013–2027.

Carpinteri, A., Ferro, G. and Invernizzi, S. (1997). The nominal tensile strength of disordered materials: a statistical fracture mechanics approach. *Eng. Fract. Mech*. **58**, 421–435.

Carter, B.J. (1992). Size and stress gradient effects on fracture around cavities. *Rock Mech. Rock Eng*. **25**, 167–186.

Clatworthy, D.E., Sellers, E.J. and Scheele, F. (1993). Investigation of splitting tensile test. Report No. 225, FRD/UCT Centre for research in computational and applied mechanics, University of Cape Town.

Colback, P.S.B. (1966). An analysis of brittle fracture initiation and propagation in the Brazilian test. Proceedings of the first Congress of the International Society of Rock Mechanics. Lisbon, 385–391.

Couvreur, J.-F. (1997). Ultrasonic wave propagation in sedimentary rocks: signal processing related to the failure process (in French). PhD thesis Université Catholique de Louvain, Louvain-la-Neuve.

Crawford, A.M. and Curran, J.H. (1982). Higher-order functional variation displacement discontinuity elements. *Int. J. Rock Mech. Min*. **19**, 143–148.

Crouch, S.L. and Starfield, A.M. (1983). Boundary elements in solid mechanics. Allen & Unwin, London, 322pp.

de Borst, R., Pamin, J., Peerlings, R.H.J. and Sluys, L.J. (1995). On gradient-enhanced damage and plasticity models for failure in quasi-brittle and frictional materials. *Comput. Mech*. **17**, 130–141.

Fairhurst, C. (1964). On the validity of the Brazilian test for brittle materials. *Int. J. Rock Mech. Min*. **1**, 535–546.

Falls, S.D., Chow, T., Young, R.P. and Hutchins, D.A. (1991). Acoustic emission analysis and ultrasonic velocity imaging in the study of rock failure. Acoustic emission: current practice and future directions, ASTM STP 1077.

Hondros, G. (1959). The evaluation of Poisson's ratio and the modulus of materials of a low tensile resistance by the Brazilian (indirect tensile) test with particular reference to concrete. *Aust. J. Appl. Sci*. **10**, 243–268.

Hsu, N.N. and Hardy, S.C. (1978). Experiments in acoustic emission waveform analysis for characterization of AE-sources. In Elastic waves and nondestructive testing of materials, AMD 29 (Edited by Y.H. Pao). ASME, New York, pp. 85–106.

Hudson, J.A., Brown, E.T. and Rummel, F. (1972). The failure of rock discs and rings loaded in diametral compression. *Int. J. Rock Mech. Min*. **9**, 241–248.

Lajtai, E.Z. (1972). Effect of tensile stress gradient on brittle fracture initiation. *Int. J. Rock Mech. Min*. **9**, 569–578.

Lavrov, A.V. and Vervoort, A. (2002). Theoretical treatment of tangential stress effects on stress distribution in Brazilian test. *Int. J. Rock Mech. Min*. 39(2), 275–283.

Malan, D.F. and Napier, J.A.L. (1995). Computer modelling of granular material microfracturing. *Tectonophysics* **248**, 21–37.

Martin, C.D. (1997). Seventeenth Canadian Geothechnical Colloquium: the effect of cohesion loss and stress path on brittle rock strength. *Can. Geotech. J*. **34**, 698–725.

Mellor, M. and Hawkes, I. (1971). Measurement of tensile strength by diametral compression of discs and annuli. *Eng. Geol*. **5**, 173–225.

Napier, J.A.L. (1990). Modelling of fracturing near deep level gold mine excavations using a displacement discontinuity approach. In Proceedings of the International Conference of the Mechanics of jointed and faulted Rocks (Edited by H.-P. Rossmanith), pp. 709–715.

Napier, J.A.L. and Hildyard, M.W. (1992). Simulation of fracture growth around openings in highly stressed brittle rock. *J. S. Afr. Inst. Min. Metall*. **92**, 159–168.

Napier, J.A.L. and Malan, D.F. (1997). A viscoplastic discontinuum model of time-dependent fracture and seismicity effects in brittle rock. *Int. J. Rock Mech. Min*. **34**, 1075–1089.

Napier, J.A.L. and Peirce, A.P. (1995). Simulation of extensive fracture formation and interaction in brittle materials. In Proceedings of the second international conference on mechanics of jointed and faulted rock (Edited by H.-P. Rossmanith), pp. 63–74.

Napier, J.A.L., Daehnke, A., Dede, T., Hildyard, M.W., Kuijpers, J.S., Malan, D.F., Sellers, E.J. and Turner, P.A. (1997). Quantification of stope fracture zone behaviour in deep level gold mines. *J. S. Afr. Inst. Min. Metall*. **97**, 119–134.

Nesetova, V. and Lajtai, E.Z. (1973). Fracture from compressive stress concentrations around elastic flaws. *Int. J. Rock Mech. Min*. **10**, 265–284.

Pijaudier-Cabot, G. and Bažant, Z.P. (1988). Nonlocal damage theory. *J. Eng. Mech. ASCE* **113**, 1512–1533.

Sellers, E.J. (1999). Review of theories of scaling and size effect in rock. Interim report for SIMRAC project GAP 601No 99–0258, CSIR: Mining Technology, Johannesburg.

Swan, G. (1980). Fracture stress scale effects for rocks in bending. *Int. J. Rock Mech. Min*. **17**, 317–324.

Van de Steen, B. (2001). Effect of heterogeneities and defects on the fracture pattern in brittle rock. PhD thesis, Katholieke Universiteit Leuven, Leuven.

Van de Steen, B. and Vervoort, A. (2001). Non-local stress approach to fracture initiation in laboratory experiments with a tensile stress gradient. *Mech. Mater*. **33**, 729–740.

Van de Steen, B., Vervoort, A. and Sahin, K. (2002). Influence of the internal structure of crinoidal limestone on fracture paths. *Eng. Geol*. **67**, 109–125.